

# Chapter 3

## Vanadium Oxide Cluster Anions

### 3.1 Introduction

In the 50's, the diatomic VO molecule was studied since its near infrared emission spectrum was found in the spectra of M-type stars [88, 89]. Dyke et al. [90] studied the photoelectron spectroscopy and Harrington and Weisshaar [91] the pulsed field ionization of VO, accessing the electronic state and vibrational frequency of  $\text{VO}^+$ . Stimulated by mass spectrometric studies [92, 93], which had found  $\text{V}_4\text{O}_{10}$  and  $\text{V}_4\text{O}_8$  as prominent vapor species above heated vanadium pentoxide, Beattie et al. in 1978 [94] observed two strong absorptions at 1030 and 828  $\text{cm}^{-1}$  in the infrared matrix absorption spectrum of  $\text{V}_2\text{O}_5$  vapor codeposited with  $\text{N}_2$  and assigned them, in analogy to  $\text{P}_4\text{O}_{10}$ , to the terminal ( $\text{V}=\text{O}$ ) and bridge ( $\text{V}-\text{O}-\text{V}$ ) modes, respectively, of neutral  $\text{V}_4\text{O}_{10}$ . The vibrational spectroscopy of other isolated polyatomic vanadium oxide species, neutral or ionic remained unexplored, until the infrared matrix absorption studies by Andriew and coworkers on  $\text{VO}_2$ ,  $\text{VO}_4$ , and  $\text{V}_2\text{O}_{2-4}$  in 1997 [95].

One of the first experimental gas phase studies on negative ions of vanadium oxide cluster was performed by Rudnyi et al., who unexpectedly detected the negative ions  $\text{VO}_2^-$ ,  $\text{VO}_3^-$ ,  $\text{V}_2\text{O}_5^-$ ,  $\text{V}_3\text{O}_8^-$  and  $\text{V}_4\text{O}_{10}^-$  in the vapor of vanadium oxide at temperatures of 1200–1500 K, hinting at a particular high stability of these vanadium oxide anions towards dissociation as well as electron detachment [96]. Collision induced dissociation studies by Bell et al. [97] on vanadium oxide cluster anions produced by laser ablation of a vanadium rod supported these results. In general, dissociation rather than electron detachment was observed and the same building blocks ( $\text{VO}_2$ ,  $\text{VO}_3$ , and  $\text{V}_2\text{O}_5$ ), were found as before for the cations. However, the average oxygen content was found to be higher and evidence was presented for higher adsorption energies for molecular oxygen in the negative ions. Dinca et al. [98] and later Bell and Castleman [99] studied the reactivity of smaller vanadium oxide cluster anions with various hydrocarbons and found a decreasing reactivity with cluster size. In partic-

ular,  $V_3O_8^-$  and  $V_4O_{10}^-$  did not react, indicating particularly stable structures for structures containing fully coordinated V atoms. Spectroscopic studies on vanadium oxide anions aiming at characterizing their structure remain scarce. Anion photoelectron spectroscopy has been used to measure electron detachment energies of mono- and divanadium oxide cluster anions as well as larger, oxygen-deficient cluster anions [100–102]. Some of the oxygen-rich vanadium oxide clusters were found to have exceptionally high electron affinities [103] ( $>5$  eV). Vyboishchikov and Sauer [103] were the first to characterize the structure and detachment energies of smaller  $V_nO_m^-$  anions (up to  $n=4$  and  $m=11$ ) employing density functional theory. They predicted stable, caged structures, which were recently spectroscopically identified by Asmis et al. [104] using IR-PD.

Attempts to predict structures from observed reactivity patterns or collision induced dissociation experiments on vanadium oxide clusters [105, 106], for example, are in conflict with later quantum chemical calculations [103, 107–112] as well as experiments [104, 113]. Reliable structure prediction is especially difficult in systems containing transition metal atoms with partially filled d-shells, because partially filled electronic d-shells leads to a manifold of structural and electronic isomers of similar total energy. Several computational studies on smaller vanadium oxide cations, for example, disagreed on the lowest electronic state and the global minimum structure, even though they applied very similar computational techniques [107, 108, 114–116]. For neutral vanadium oxide clusters, Matsuda and Bernstein [117] predicted closed shell singlet ground states for systems with an even number of electrons, which is in conflict with previous calculations [109, 110]. Therefore the reliable identification of the cluster structure generally requires the confirmation by experimental data, e.g., from vibrational spectroscopy.

The central aim of this work is to characterize the vibrational spectroscopy of smaller vanadium oxide cluster anions in order to elucidate the evolution of their structure with size by a combined experimental / computational approach. IR-PD spectra of mass-selected vanadium oxide cluster anions, from  $V_2O_6^-$  to  $V_8O_{20}^-$ , are compared with DFT electronic structure calculations carried out in the Sauer group (Humboldt-Universität zu Berlin, Germany). DFT calculations were done using the TURBOMOLE program [118], employing the B3LYP hybrid functional [119] and the TZVP basis sets [120]. Calculated stick spectra (in this and in all following chapters) are convoluted with a Gaussian line shape of  $20\text{ cm}^{-1}$  FWHM for better comparison with the experimental spectra.

## 3.2 Experimental Details

The vanadium oxide clusters are prepared by laser vaporization (see Section 2.1) operated at 20 Hz. A mixture of 1.5%  $O_2$  seeded in helium as carrier gas is used. A

typical mass spectrum is shown in Figure 3.1. The infrared photodissociation (IR-PD) spectra (according to equation (1.7)) are recorded by monitoring the fragment formation in dependence on the FELIX wavelength. In order to check the stability of the source conditions, the parent ion yield is measured once at the beginning and once at the end of each wavelength step. Its variations are typically on the order of 10%. The fragment ion yield is less than 5% of the parent yield for the smaller anions, and increases with cluster size up to more than 80% for the  $V_8O_{20}^-$ , the larger cluster studied. Generally, possible fragment ions are determined by measuring an “on-resonance” fragment ion mass spectrum with FELIX at full power tuned to the vanadyl absorption band at 10  $\mu\text{m}$  and scanning the second mass filter. Then, an overview spectrum is first measured in the region from 6 to 17  $\mu\text{m}$  with a step size of 0.1  $\mu\text{m}$ , monitoring different fragments. Spectra with smaller step sizes are then measured for the fragment ions of interest. During one spectral scan, up to four ions of different mass are monitored. The experiments on the smaller cluster ions are performed using the ZnSe setup, while the experiments on the larger ones ( $V_5O_{13}^-$ ,  $V_6O_{15}^-$ ,  $V_7O_{18}^-$ , and  $V_8O_{20}^-$ ) are performed with the KRS-5 setup (see Section 2.2). All IR-PD spectra shown here are not corrected for this transmission dependence, because this would require the knowledge of the cross section of the individual absorption processes comprising the sequential multiple photon absorption process. The accuracy of the determined vibrational frequencies is generally within 1% of the central wavelength.

### 3.3 Results

A typical, low-resolution mass spectrum of vanadium oxide cluster anions formed by laser ablation is shown in Figure 3.1. The spectrum extends from mass to charge ratios of 150 to 800 amu. The observed group of peaks are assigned to vanadium oxide cluster anions  $V_xO_y^-$  with  $x=2$  to 8. A relatively high concentration of oxygen is used in the gas pulse, leading to high oxygen atom-vanadium atom ratios ranging between two and four. A ratio of 2.5 indicates fully oxidized vanadium, i.e., formal oxidation number of +5 on vanadium atoms and  $-2$  on oxygen atoms. Ratios above 2.5 signal the presence of per- or super-oxides. The ratio can be tuned by changing the oxygen concentration and the measurement of the IR-PD spectra was performed with a lower concentration.

IR-PD spectra of vanadium oxide cluster anions are measured for cluster sizes between  $V_2O_6^-$  and  $V_8O_{20}^-$ . An overview of the IR-PD spectra is shown in the left column of Figure 3.2. For many parent ions multiple fragmentation channels are observed, producing signal at different fragment ion masses. All observed fragmentation channels and experimental band positions are listed in Table 3.1. In most cases the IR-PD spectra of a specific parent ion measured at different fragment ion masses are

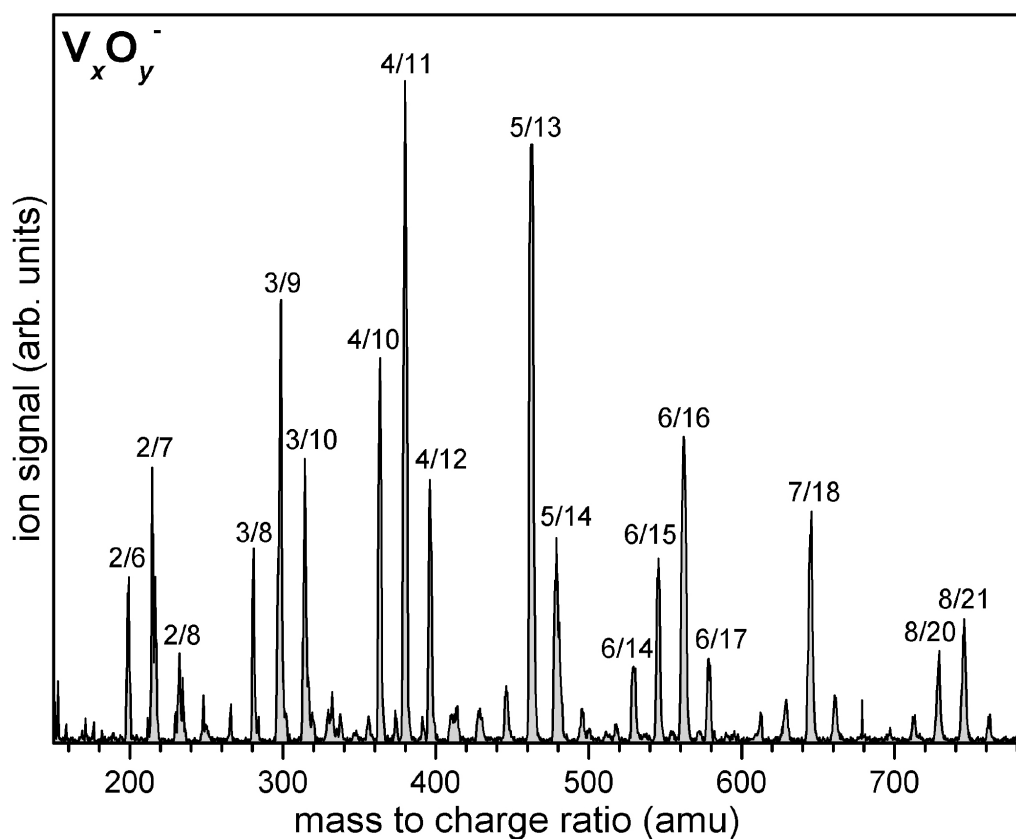


**Figure 3.1:** Mass spectrum of vanadium oxide cluster anions produced by laser vaporization.

very similar and therefore only the spectrum of the most abundant fragment ion is shown. In some cases, however, different fragmentation channels produce different IR-PD spectra and these are shown in more detail in separate figures. No photodissociation is observed for the vanadium oxide anions smaller than  $V_2O_6^-$ , presumably due to the decreasing efficiency of the multiphoton absorption with decreasing cluster size.

Simulated linear absorption spectra of the lowest energy isomer in its electronic ground state are used to aid in the structural assignment and are shown in the right column of Figure 3.2. The simulated linear absorption spectra were generated by convoluting stick spectra, based on B3LYP/TZVP scaled harmonic frequencies and oscillator strengths [121], with a Gaussian line function.

$V_2O_6^-$  O-atom abstraction and formation of  $V_2O_5^-$  is the only fragmentation channel observed upon irradiation of  $V_2O_6^-$  with FELIX. Photodissociation producing

Parent Ion	Fragment Ion	Position of Observed Bands ( $\text{cm}^{-1}$ )
$\text{V}_2\text{O}_6^-$	$\text{V}_2\text{O}_5^-$	$\sim 975(\text{s}), 959, 930, 911, 888, 800, 775, 738, (\sim 620)$
$\text{V}_2\text{O}_7^-$	$\text{V}_2\text{O}_5^-$	1112, 987, $\sim 965(\text{s}), 952, 775, 705, 627$
$\text{V}_3\text{O}_8^-$	$\text{V}_3\text{O}_7^-$ $\text{V}_2\text{O}_5^-$ $\text{VO}_3^-$	964, 922, 826, 715(s), 680, 651(s)
$\text{V}_4\text{O}_{10}^-$	$\text{V}_3\text{O}_8^-$	990, 670(s), 637, 602
$\text{V}_4\text{O}_{11}^-$	$\text{V}_4\text{O}_{10}^-$ $\text{V}_3\text{O}_8^-$	999, 990(s), 976(s), 899(s), 874(s), 824, 785(s), 721, 648 988, 976(s), 865(s), 832(s), 810, 728
$\text{V}_5\text{O}_{13}^-$	$\text{V}_3\text{O}_8^-$ $\text{V}_4\text{O}_{10}^-$ $\text{V}_5\text{O}_{12}^-$	1000, 948, 900(s), 843 1000, 948(s), 906(s), 884 (s), 843 1002, 854
$\text{V}_6\text{O}_{15}^-$	$\text{V}_3\text{O}_8^-$ $\text{V}_4\text{O}_{10}^-$ $\text{V}_5\text{O}_{13}^-$	962, 830 971, 830 972, 830
$\text{V}_7\text{O}_{18}^-$	$\text{V}_3\text{O}_8^-$ $\text{V}_4\text{O}_{10}^-$ $\text{V}_5\text{O}_{13}^-$ $\text{V}_6\text{O}_{15}^-$	1004, 871 994, 859 1001, 877, 925(s) 1012, 869, 807(s), 739
$\text{V}_8\text{O}_{20}^-$	$\text{V}_4\text{O}_{10}^-$ $\text{V}_3\text{O}_8^-$ $\text{V}_5\text{O}_{13}^-$	1004, 871

**Table 3.1:** Experimental vibrational frequencies (in  $\text{cm}^{-1}$ ) of vanadium oxide cluster anions determined from the respective IR-PD spectra, measured monitoring fragment ion mass-selectively. Vibrational frequencies are determined from band maxima or estimated based on observable shoulders (s) formed by overlapping transitions.

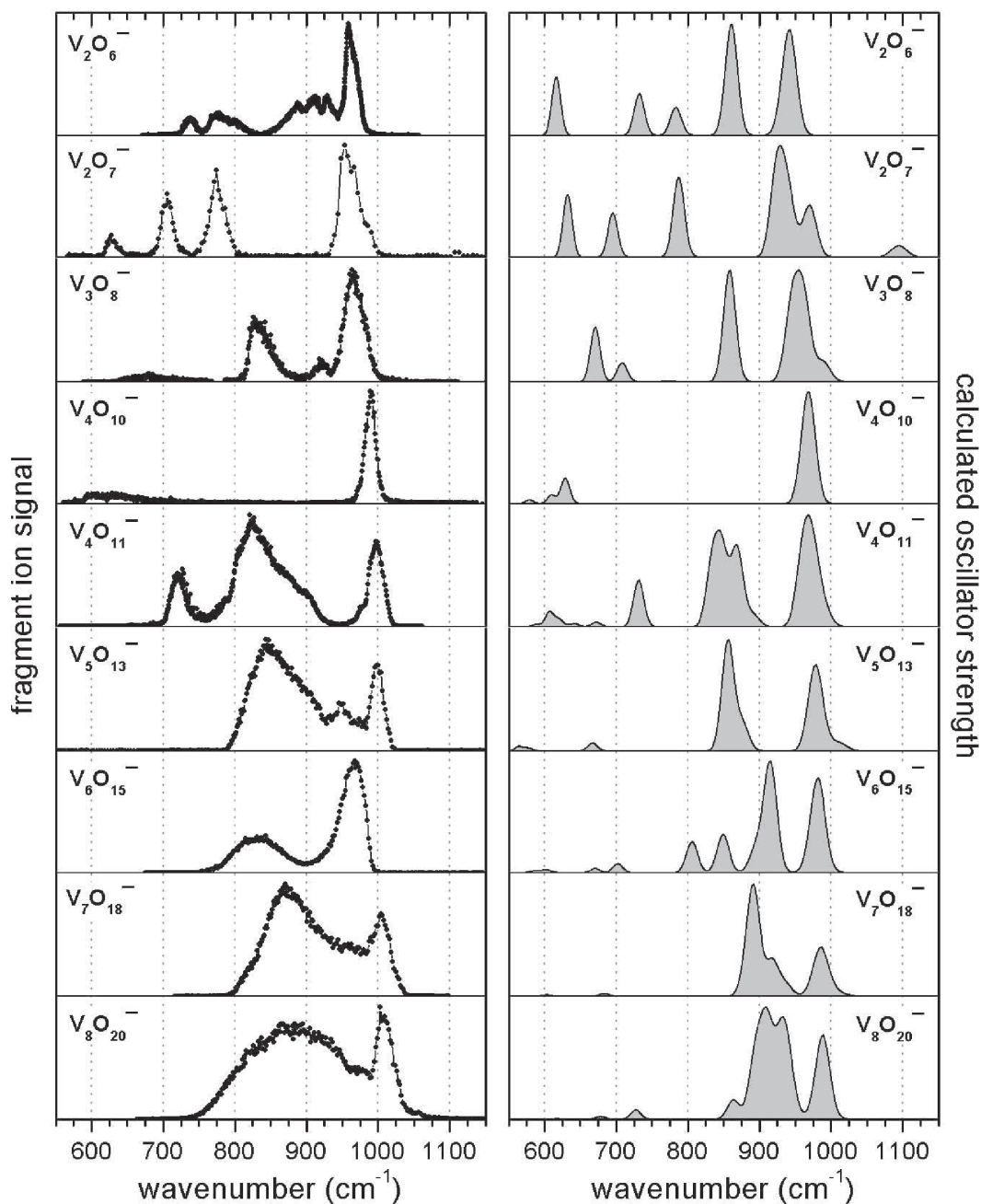


**Figure 3.2:** Experimental IR-PD spectra (left column) and simulated IR absorption spectra (right column), based on scaled B3LYP/TZVP frequencies and oscillator strengths of the lowest energy isomer in its electronic ground state of vanadium oxide cluster anions ranging from for  $V_2O_6^-$  to  $V_8O_{20}^-$  (from top to bottom).

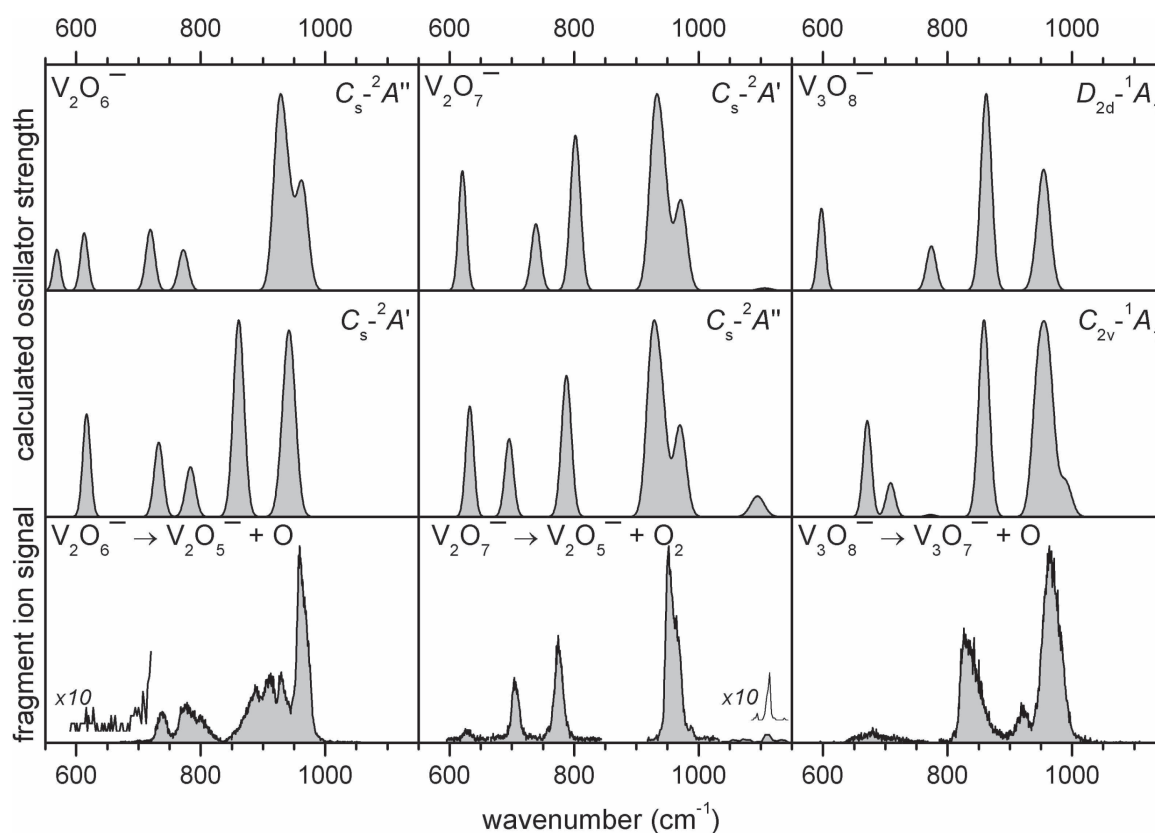


**Figure 3.3:** Simulated IR absorption spectra, based on scaled B3LYP/TZVP frequencies and oscillator strengths of the lowest energy isomer in its electronic ground state (middle row) and an energetically low-lying isomer (top row) for  $V_2O_6^-$ ,  $V_2O_7^-$ , and  $V_3O_8^-$  (from left to right). The lower row shows the experimental IR-PD spectra.

$VO_3^-$  ( $VO_3$  loss channel), observed in CID studies [97] at high collision energies, is not detected under the present conditions. The IR-PD spectrum of  $V_2O_6^-$  (see Figure 3.3), measured by monitoring the  $V_2O_5^-$  fragment ion yield as a function of FELIX photon energy, is complex and reveals at least eight bands in-between 550 and  $1150\text{ cm}^{-1}$ . The most intense feature at  $959\text{ cm}^{-1}$  is slightly asymmetric; the shoulder on its high energy tail indicates a second, overlapping band at  $970\text{ cm}^{-1}$ . At slightly lower photon energies a broader feature extending from  $945$  to  $835\text{ cm}^{-1}$  with three distinct maxima at  $930$ ,  $911$  and  $888\text{ cm}^{-1}$  is observed. Another three partially overlapping bands are found at  $800$ ,  $775$  and  $738\text{ cm}^{-1}$ . A very weak signal centered around  $620\text{ cm}^{-1}$  and roughly twice as large as the background signal is tentatively assigned to an additional transition. Note, that above  $15\text{ }\mu\text{m}$  (i.e., below  $670\text{ cm}^{-1}$ ) the transmission of the ZnSe optic decreases substantially, leading to a decrease in the relative band intensities in this spectral region.

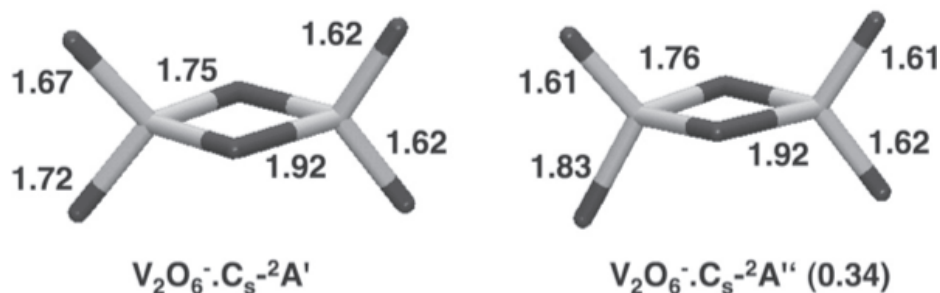


**Figure 3.4:** B3LYP/TZVP optimized structures for  $V_2O_6^-$ . The lowest energy isomer (left) and an energetically low-lying isomer (right). Bond lengths are in Å and relative energy (in parenthesis) with respect to the ground state is in eV.

The lowest energy structure found for  $V_2O_6^-$ , shown in Figure 3.4, has  $C_s$  symmetry and consists of a four-membered V–O–V–O ring plus two singly-coordinated oxygen atoms on each V atom. Localization of the unpaired electron on one of the terminal O atoms leads to a pronounced asymmetry in the lengths of the terminal V–O bonds (1.62 Å and 1.72 Å) as well as the ring V–O bonds (1.75 and 1.92 Å). The simulated vibrational spectrum (see Figure 3.3) consists of a total of six vibrational transitions. The three characteristic “in-plane” normal modes of the central four-membered V–O–V–O ring known from the  $V_2O_m^+$  cation spectra [113] are predicted at 617, 733, and 783  $cm^{-1}$  and assigned to the bands at  $\sim 620$ , 738, and 775  $cm^{-1}$ . The symmetric and antisymmetric V=O bonds (1.62 Å) at 944 and 937  $cm^{-1}$  are assigned to the strong band observed at 975  $cm^{-1}$ . The two terminal V–O bonds with a length of 1.72 Å give rise to a symmetric stretch vibration that might be assigned to one of the triplet of peaks observed at 930, 911, and 888  $cm^{-1}$ . The simulated vibrational spectrum of the  ${}^2A'$  ( $C_s$ ) structure of  $V_2O_6^-$  agrees reasonably well with the experimental IR-PD spectrum with respect to the band positions; in particular the agreement is better than for the next lowest electronic state of  ${}^2A''$  symmetry (see Figure 3.3). The differences with respect to the relative intensities of the vibrational transitions in the experimental and the simulated spectrum are in part caused by the reduced transmission of the ZnSe optics at longer wavelengths ( $>15 \mu m$ ) and consequently a pronounced decrease of the efficiency of the multiple photon dissociation mechanism, in particular for smaller cluster anions. The presence of multiple isomers ( ${}^2A'$  and  ${}^2A''$ ) in the trap is also possible, but improbable in this particular case, as the  ${}^2A''$  state is calculated more than 30 kJ/mol above the  ${}^2A'$  ground state.

**$V_2O_7^-$**  Photodissociation of  $V_2O_7^-$  leads exclusively to formation of  $V_2O_5^-$ , also with a strongly attenuated FELIX beam, hinting at the loss of molecular oxygen rather than two oxygen atoms. Evidence for  $O_2$  loss was also found in the previous CID study [97]

and is in agreement with the calculated fragmentation energies (see Table 3.2). Further support is found in the IR-PD spectrum of  $V_2O_7^-$  (see Figure 3.3). A very weak (and narrow) band, the O=O stretching mode of a superoxo-group, is observed at  $1112\text{ cm}^{-1}$ . The vanadyl band slightly below  $1000\text{ cm}^{-1}$  is the largest feature in the spectrum and is made up of multiple transitions. Based on IR-PD spectra measured at various laser powers (Figure 3.5), three transitions are found at  $952\text{ cm}^{-1}$  (absolute maximum),  $\sim 965\text{ cm}^{-1}$  (shoulder) and  $987\text{ cm}^{-1}$  (relative maximum), suggesting three V=O oscillators. The three bands below  $800\text{ cm}^{-1}$ , at  $775$ ,  $705$  and  $627\text{ cm}^{-1}$ , are assigned to V–O–V modes.

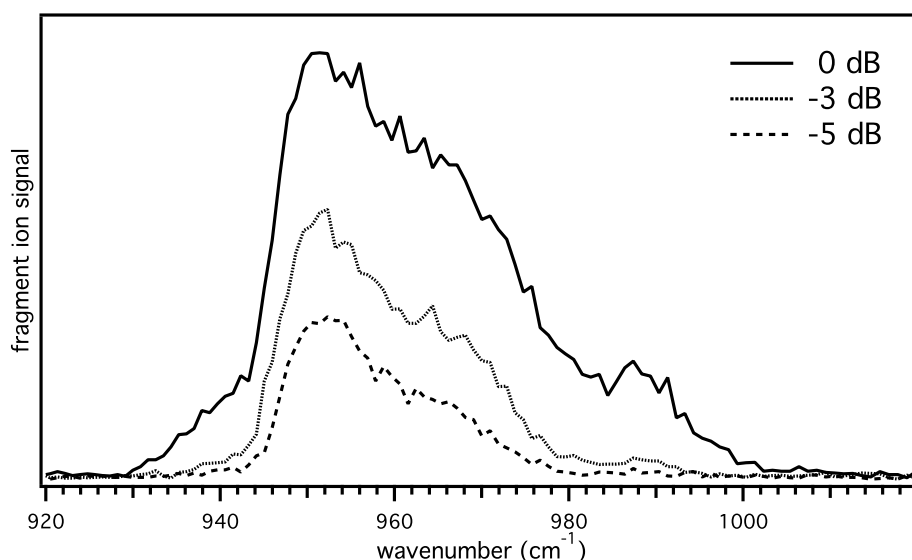


**Figure 3.5:** IR-PD spectra of  $V_2O_7^-$  in the  $920$  to  $1020\text{ cm}^{-1}$  region, measured with different FELIX attenuations.

The lowest energy isomer found for  $V_2O_7^-$  has a  $V_2O_6^-$ -like structure of  $C_s$  symmetry, in which a terminal oxygen atom is replaced by a superoxo-unit (see Figure 3.6). Satisfactory agreement between experimental and simulated peak positions is found, supporting the above assignment to one superoxo mode, calculated at  $1095\text{ cm}^{-1}$ , three modes involving different combinations of the symmetric stretching motion along the three vanadyl bonds ( $970$ ,  $940$  and  $925\text{ cm}^{-1}$ ) and the three characteristic V–O–V–O ring modes ( $788$ ,  $696$  and  $632\text{ cm}^{-1}$ ). The deviation in intensity of the  $627\text{ cm}^{-1}$  band may be attributed to the same mechanism as indicated for  $V_2O_6^-$ . The next lowest energy isomer (Figure 3.6) ( $C_s^{-2}A'$ ) is more than  $50\text{ kJ/mol}$  higher in energy and its calculated spectrum agrees less satisfactorily with the IR-PD spectrum (see Figure 3.3).

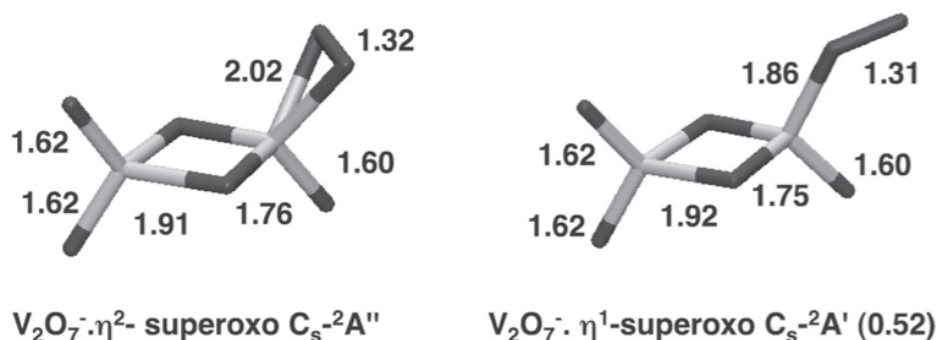


**Figure 3.6:** B3LYP/TZVP optimized structures for  $\text{V}_2\text{O}_7^-$ . The lowest energy isomer (left) and an energetically low-lying isomer (right). Bond lengths are in Å and relative energy (in parenthesis) with respect to the ground state is in eV.

$\text{V}_3\text{O}_8^-$  Upon photodissociation of  $\text{V}_3\text{O}_8^-$  three photofragment ions are observed:  $\text{V}_3\text{O}_7^-$  (O-atom loss),  $\text{V}_2\text{O}_5^-$  ( $\text{VO}_3$  loss) and  $\text{VO}_3^-$  ( $\text{V}_2\text{O}_5$  loss). All three fragment ions yield similar IR-PD spectra. The dominant photofragmentation process is atomic oxygen loss, followed by  $\text{VO}_3$  loss and  $\text{V}_2\text{O}_5$  loss with relative yields of 1, 0.1, and 0.05, respectively. This is in qualitative agreement with calculated fragmentation energies (Table 3.2) which also favor atomic oxygen loss. Interestingly, the CID experiments by Castleman and coworkers [97] show the formation of  $\text{VO}_3^-$ ,  $\text{V}_2\text{O}_5^-$  and  $\text{V}_2\text{O}_6^-$  fragment ions. They do not observe O-atom loss, whereas in the present experiments no evidence is found for the formation  $\text{V}_2\text{O}_6^-$ .

The IR-PD spectrum of  $\text{V}_3\text{O}_8^-$  (O-atom loss channel) is shown in Figure 3.3. Four features are observed. The two strongest bands, at  $964 \text{ cm}^{-1}$  and  $825 \text{ cm}^{-1}$ , are considerably broader than the FELIX bandwidth, suggesting that multiple, overlapping transitions contribute to the band profile. The same holds for the broad feature extending from  $770 \text{ cm}^{-1}$  down to  $640 \text{ cm}^{-1}$  with a maximum at  $680 \text{ cm}^{-1}$  and two shoulders at  $715 \text{ cm}^{-1}$  and  $651 \text{ cm}^{-1}$ . A more narrow band is found at  $922 \text{ cm}^{-1}$ .

The lowest energy structure predicted for  $\text{V}_3\text{O}_8^-$ , the closed-shell  $^1A_1$  ground state, is bicyclic with  $C_{2v}$  symmetry (see Figure 3.7). A chain-like  $D_{2d}$  structure is found 0.46 eV higher in energy. Comparison of the experimental and simulated spectra, in particular in the  $580$  to  $800 \text{ cm}^{-1}$  region, clearly favors the bicyclic geometry, in agreement with the calculated energetics. The most intense band in the IR-PD spectrum at  $964 \text{ cm}^{-1}$  is assigned to the four vanadyl modes. All bands observed below  $900 \text{ cm}^{-1}$  are assigned to V–O–V ring modes. The mode calculated at  $859 \text{ cm}^{-1}$  ( $826 \text{ cm}^{-1}$  band) involves motion of atoms comprising the six-membered ring, while the  $671 \text{ cm}^{-1}$  mode ( $680 \text{ cm}^{-1}$  band) is localized more on the four-membered ring. The other modes involve more complex deformations. The peak at  $922 \text{ cm}^{-1}$  is reproduced in neither of the two simulated spectra and remains unassigned.

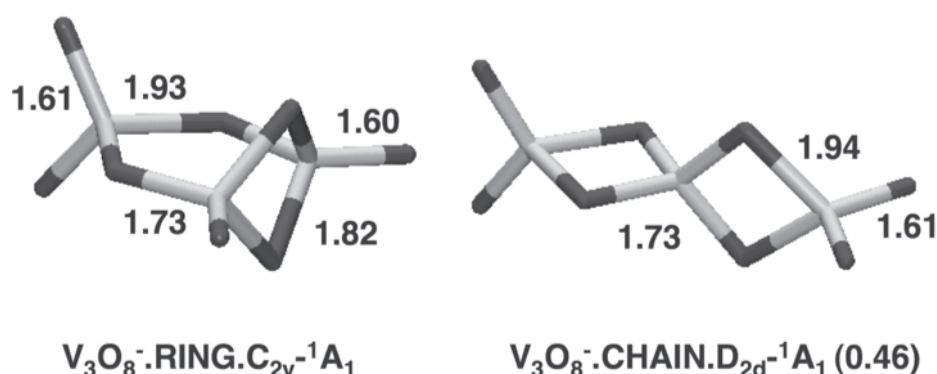


**Figure 3.7:** B3LYP/TZVP optimized structures for  $\text{V}_3\text{O}_8^-$ . The lowest energy isomer (left) and an energetically low-lying isomer (right). Bond lengths are in Å and relative energy (in parenthesis) with respect to the ground state is in eV.

$\text{V}_4\text{O}_{10}^-$  A single photofragment channel, dissociation to  $\text{V}_3\text{O}_8^- + \text{VO}_2$ , is observed upon photodissociation of  $\text{V}_4\text{O}_{10}^-$ . The same dissociation channel is also found in the recent CID experiments [97]. The IR-PD spectrum of  $\text{V}_4\text{O}_{10}^-$  (see Figure 3.2) looks intriguingly simple. Two features are observed in the spectrum; an intense, narrow and slightly asymmetric peak at  $990 \text{ cm}^{-1}$  and a group of weak, overlapping bands extending from  $750$  to  $575 \text{ cm}^{-1}$ , with maxima at  $637$  and  $602 \text{ cm}^{-1}$  and a weak shoulder at  $670 \text{ cm}^{-1}$ . The presence of only a single, rather narrow band in the spectral region of the vanadyl stretches ( $>900 \text{ cm}^{-1}$ ) and the absence of any significant absorption in-between  $750$  to  $950 \text{ cm}^{-1}$  suggests a highly symmetrical structure for  $\text{V}_4\text{O}_{10}^-$ .

For  $\text{V}_4\text{O}_{10}^-$  a tetragonal  $D_{2d}$  structure (Figure 3.8) is found which is minimally Jahn-Teller distorted from the  $T_d$  structure. The electronic ground state is  ${}^2\text{B}_1$ . The unpaired electron is fully delocalized about all four symmetry-equivalent, fourfold-coordinated V atoms, forming one short V=O double bond ( $1.59 \text{ Å}$ ) and three V–O single bonds ( $1.81 \text{ Å}$ ). The four vanadyl stretches combine to one totally-symmetric mode  $a_1$  which is IR-inactive and three IR-active  $e$  and  $b_2$  modes which are quasi-degenerate and form the single narrow band at  $969 \text{ cm}^{-1}$  in the simulated spectrum that corresponds to the  $990 \text{ cm}^{-1}$  peak in the experimental IR-PD spectrum. The six symmetric V–O–V bond stretches also give rise to three IR active  $e$  and  $b_2$  modes ( $629$  and  $609 \text{ cm}^{-1}$ , respectively). They have a cumulative oscillator strength that is about  $1/3$  of the vanadyl bands, in good agreement with experiment. The modes resulting from the six antisymmetric V–O–V bond stretches are found below  $600 \text{ cm}^{-1}$  and have vanishing intensities.

$\text{V}_4\text{O}_{11}^-$  IR-PD of  $\text{V}_4\text{O}_{11}^-$  leads to formation of  $\text{V}_4\text{O}_{10}^-$  (O-atom loss) and  $\text{V}_3\text{O}_8^-$  ( $\text{VO}_3$  loss), respectively. These two ionic products were also observed in the previous

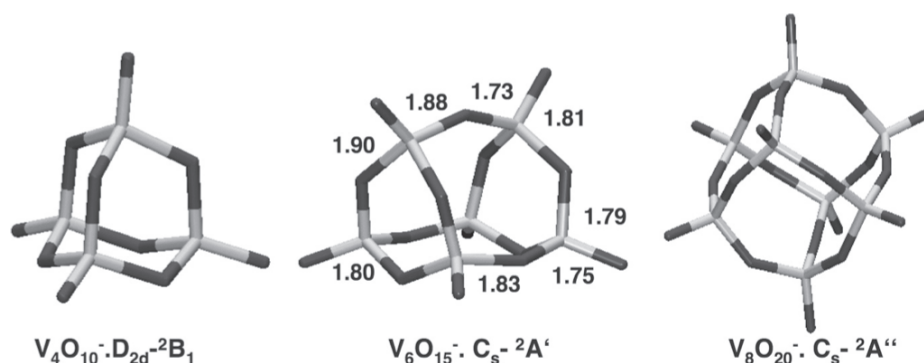


**Figure 3.8:** B3LYP/TZVP optimized structures for  $V_4O_{10}^-$ ,  $V_6O_{15}^-$ , and  $V_8O_{20}^-$ . Bond lengths are in Å.

CID studies [97]. O-atom loss is favored, in agreement with calculated B3LYP/TZVP reaction energies of 2.05 eV (O loss) and 3.95 eV ( $VO_3$  loss) for the fragmentation channels. The IR-PD spectrum of  $V_4O_{11}^-$  (O loss) is shown in Figure 3.9. It reveals three bands at 999, 824 and  $721\text{ cm}^{-1}$  and multiple shoulders, indicating at least eight transitions in this region of the spectrum. In particular the strong absorption in the  $950$  to  $750\text{ cm}^{-1}$  region makes it qualitatively different from the much simpler  $V_4O_{10}^-$  IR-PD spectrum; a trend that is continued through the IR-PD spectra of the larger cluster anions. On the other hand, the position and width of the vanadyl band remains similar in the IR-PD spectra of all cluster anions studied here. Monitoring  $V_3O_8^-$  fragment ions instead of the  $V_4O_{10}^-$  yields an IR-PD spectrum (see Figure 3.9) with ion signal in the same spectral region, however, with significantly different relative intensities and slightly shifted peak positions. The fragment ion ratio  $I(V_4O_{10}^-)/I(V_3O_8^-)$  increases from roughly 3/1 at  $988\text{ cm}^{-1}$  to over 50/1 in the  $V_3O_8^-$  fragment ion IR-PD spectrum at the position of the lowest band ( $722\text{ cm}^{-1}$ ). This can be rationalized assuming a sequential fragmentation process involving  $V_4O_{10}^-$  as an intermediate fragment ion. First an oxygen atom is lost, then (vibrationally hot)  $V_4O_{10}^-$  continues to absorb photons until eventually  $VO_2$  is lost forming  $V_3O_8^-$  as a final product. The cross section for formation of  $V_3O_8^-$  in such a sequential mechanism will then also reflect the absorption cross section of  $V_4O_{10}^-$ . Because  $V_4O_{10}^-$  predominantly absorbs in-between  $950$ – $1020\text{ cm}^{-1}$ ,  $V_3O_8^-$  is mainly formed at these photon energies.

The best agreement between the experimental IR-PD spectrum (O loss channel) and simulated IR spectrum of six isomers of  $V_4O_{11}^-$  shown in Figure 3.10 is found for the lowest energy structure, “DIOXO-bridge”. This isomer is formally obtained from  $V_4O_{10}^-$  by replacing O in one of the V–O–V bridges by  $\mu$ -O–O (peroxo) and by subsequently opening the V–O–O–V bridge. As a result, there is a stretched ( $1.65\text{ Å}$ ) vanadyl group on one of the V sites, with the oxygen still in a “bridging”

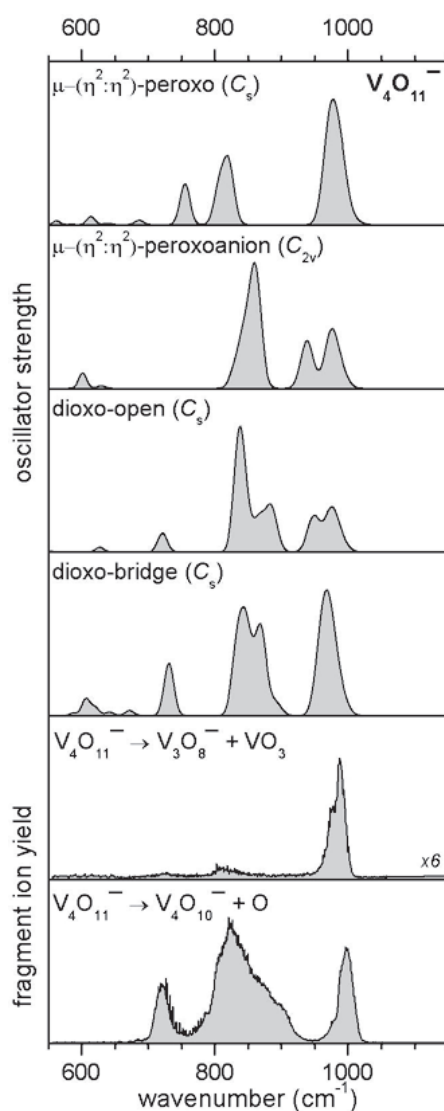


**Figure 3.9:** Simulated IR absorption spectra, based on scaled B3LYP/TZVP frequencies and oscillator strengths of low energy isomers for V<sub>4</sub>O<sub>11</sub><sup>-</sup>. The lower rows show two experimental IR-PD spectra, measured monitoring fragment ions of different masses.

position, and a terminal V–O· group with the unpaired electron on the other V site (1.75 Å). The former leads to an absorption at 868 cm<sup>-1</sup> which is the strongest in the whole spectrum, while the latter is connected with a very weak absorption at 642 cm<sup>-1</sup>. The original vanadyl groups on these V sites are slightly longer (1.60 and 1.61 Å) than in V<sub>4</sub>O<sub>10</sub><sup>-</sup> and have vibrations at 960 and 891 cm<sup>-1</sup>, respectively. The two vanadyl groups at V sites that are not affected by the additional O and vibrate at

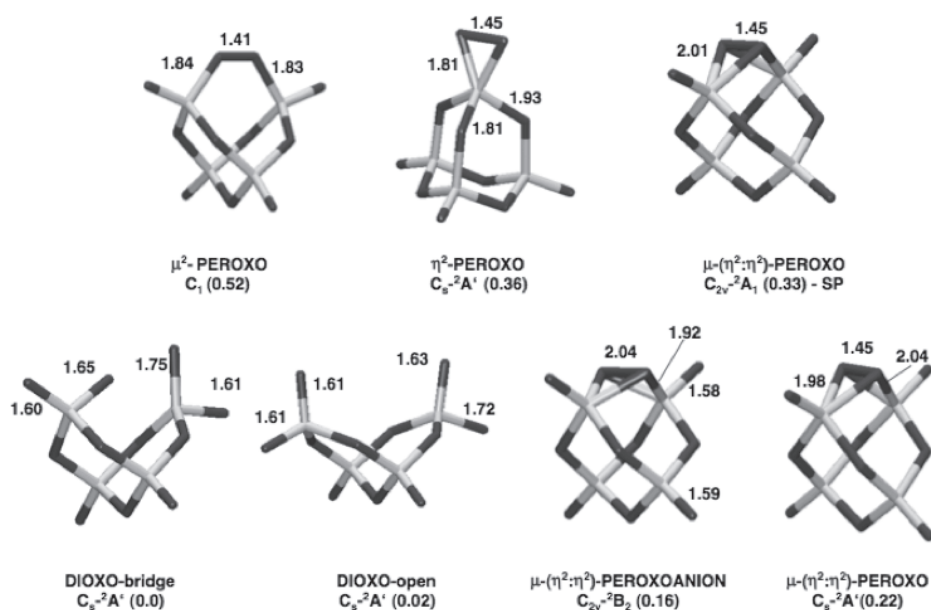


**Figure 3.10:** B3LYP/TZVP optimized structures for  $V_4O_{11}^-$ . The lowest energy isomer (bottom left) and energetically low-lying isomer. Bond lengths are in Å and relative energy (in parenthesis) with respect to the ground state is in eV.

989 (in phase) and  $973\text{ cm}^{-1}$  (out-of-phase). The very intense vibrations at  $973\text{ cm}^{-1}$  (out-of phase) and  $960\text{ cm}^{-1}$  are assigned to the features at  $999$  and  $990\text{ cm}^{-1}$  in the experimental spectrum. The weaker shoulder at  $976\text{ cm}^{-1}$  is then the in-phase combination of lower intensity, calculated at  $989\text{ cm}^{-1}$ . The experimental features observed in the  $900\text{--}800\text{ cm}^{-1}$  region are assigned to the “bridging”  $V=O$  vibration ( $868\text{ cm}^{-1}$ ) and intense  $V-O-V$  vibrations calculated at  $848$  and  $834\text{ cm}^{-1}$ . The band at  $721\text{ cm}^{-1}$  is assigned to a  $V-O-V$  mode calculated at  $732\text{ cm}^{-1}$ .

There is another dioxo-isomer, “DIOXO-open”, with a more open structure and the long  $V-O$  bond pointing away from the second dioxo site. Its calculated IR spectrum is very similar. B3LYP/TZVP predicts that the DIOXO-open isomer is only  $0.02\text{ eV}$  higher than the DIOXO-bridge. The other  $V_4O_{11}^-$  isomers in Figure 3.10 are all obtained by substituting a peroxo group for a bridging or a terminal O atom. They all have higher energies than the “DIOXO” structures and their calculated IR spectra show less agreement with the observed one (Figure 3.9).

**$V_5O_{13}^-$**  For  $V_5O_{13}^-$  three photofragments are observed:  $V_3O_8^-$  ( $V_2O_5$  loss),  $V_4O_{10}^-$  ( $VO_3$  loss) and  $V_5O_{12}^-$  (O loss). At  $843\text{ cm}^{-1}$ , the maximum of the main band in the IR-PD spectrum, the relative fragment ion yields are 1, 0.85, 0.08, respectively. The IR-PD spectra of the three fragments are similar with minor differences in the relative intensities of the individual features (see Figure 3.11). They all display a

narrow band at  $1000\text{ cm}^{-1}$  and a much broader ( $930\text{--}790\text{ cm}^{-1}$ ) and more intense feature at  $\sim 850\text{ cm}^{-1}$ . The weak band at  $948\text{ cm}^{-1}$  in the  $\text{V}_2\text{O}_5$  loss spectrum, is only observed as a shoulder in the other two spectra. The CID experiments [97] find no  $\text{V}_5\text{O}_{12}^-$  fragment ions, only  $\text{V}_3\text{O}_8^-$  and  $\text{V}_4\text{O}_{10}^-$ . This suggests, that the fragmentation to  $\text{V}_4\text{O}_{10}^-$  proceeds sequentially, via the formation of  $\text{V}_5\text{O}_{12}^-$ , and is not observed in the CID experiment, because considerably more excess energy is deposited into the parent ion compared to the present IR-PD experiment.

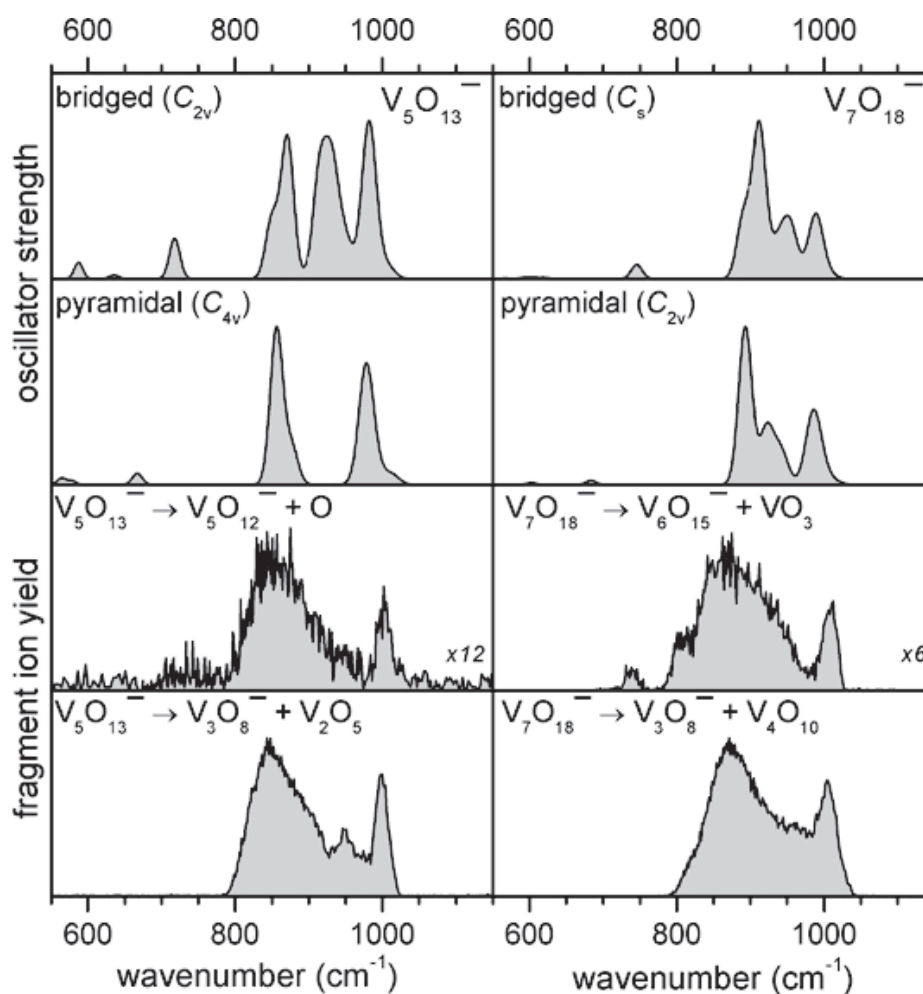


**Figure 3.11:** Simulated IR absorption spectra, based on scaled B3LYP/TZVP frequencies and oscillator strengths of the lowest energy isomer in its electronic ground state (middle row) and an energetically low-lying isomer (top row) for  $\text{V}_5\text{O}_{13}^-$  (left) and  $\text{V}_7\text{O}_{18}^-$  (right). The lower row shows two experimental IR-PD spectra for each parent ion, measured monitoring fragment ions of different masses.

The DFT calculations predict two nearly isoenergetic species for  $\text{V}_5\text{O}_{13}^-$  (see Fig-

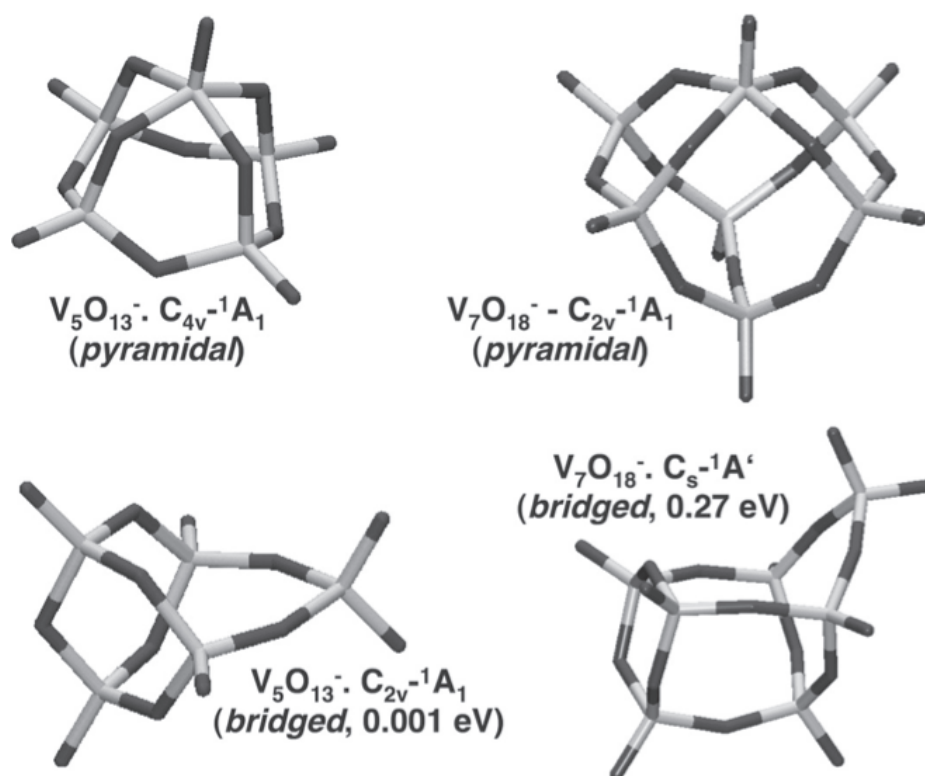


**Figure 3.12:** B3LYP/TZVP optimized structures for  $V_5O_{13}^-$  (left) and  $V_7O_{18}^-$  (right). The lowest energy isomers (bottom) and energetically low-lying isomers (top). Bond lengths are in Å and relative energy (in parenthesis) with respect to the ground state is in eV.

ure 3.12), a pyramidal  $C_{4v}$  structure and a bridged  $C_{2v}$  structure only 1 meV higher in energy. The IR absorption spectrum of the pyramidal structure is characterized by two strong absorption features at  $980\text{ cm}^{-1}$  (five  $V=O$  stretch modes) and  $860\text{ cm}^{-1}$  (four  $V-O-V$  stretch modes) and much weaker absorption below  $700\text{ cm}^{-1}$ . The bridged structure, on the other hand, is characterized by three strong absorption bands in the region above  $800\text{ cm}^{-1}$ . The third band ( $930\text{ cm}^{-1}$ ) lies in-between the  $870$  and  $980\text{ cm}^{-1}$  bands that are also observed in the first isomer. Four rather strong transitions contribute to the absorption in the  $900\text{--}960\text{ cm}^{-1}$  region, two low-lying  $V=O$  stretch modes, involving the two vanadyl bonds on the bridging vanadium atom, and two  $V-O-V$  stretching modes, localized on the ring including the bridge. The experimental IR-PD spectrum shows absorption in this region of the spectrum, however the relative intensities are different, making an assignment to either of the isomers difficult. Best agreement between experiment and theory is achieved, if both isomers are assumed to be present with a ratio of 3:1 in favor of the pyramidal structure.

**V<sub>6</sub>O<sub>15</sub><sup>-</sup>** Three photofragment channels leading to the formation of V<sub>3</sub>O<sub>8</sub><sup>-</sup> (V<sub>3</sub>O<sub>7</sub> loss), V<sub>4</sub>O<sub>10</sub><sup>-</sup> (V<sub>2</sub>O<sub>5</sub> loss), and V<sub>5</sub>O<sub>13</sub><sup>-</sup> (VO<sub>2</sub> loss) with relative yields (at 850 cm<sup>-1</sup>) of 1, 0.6, and 0.07, respectively, are observed for IR-PD of V<sub>6</sub>O<sub>15</sub><sup>-</sup>. All three spectra show the same two features, an intense, narrower band at 960–980 cm<sup>-1</sup> and a weaker, broader feature peaking at around 840 cm<sup>-1</sup>. The intense feature is characterized by a tail on its red side indicating at least one additional weaker transition at about 940–950 cm<sup>-1</sup>. The overall appearance of this IR-PD spectrum is different from the other experimental spectra of the larger clusters (>V<sub>4</sub>O<sub>10</sub><sup>-</sup>) in Figure 3.2 in that (i) the vanadyl band is red-shifted close to the position it is observed in the spectra of the smaller clusters (<V<sub>4</sub>O<sub>10</sub><sup>-</sup>) and (ii) the intensity ratio between vanadyl and V–O–V bands is shifted in favor of the vanadyl band in V<sub>6</sub>O<sub>15</sub><sup>-</sup>.

The lowest energy structure found for V<sub>6</sub>O<sub>15</sub><sup>-</sup> is a distorted cage structure with C<sub>s</sub> symmetry and a <sup>2</sup>A' electronic ground state (see Figure 3.8). Other structures of higher symmetry were found +10 kJ/mol (C<sub>2v</sub> isomer) and +44 kJ/mol (D<sub>3h</sub> isomer) higher in energy. The simulated spectrum of the C<sub>s</sub> isomer (see Figure 3.13), however, does not agree well with the experimental spectrum. In particular, the intense a' transition, calculated at 915 cm<sup>-1</sup>, is not observed in the experimental spectrum. A closer look at this particular vibrational mode reveals that it is anharmonic in nature. There actually exist two equivalent C<sub>s</sub> structures, which are connected through a C<sub>2v</sub> transition state by a <sup>2</sup>A<sub>2</sub> saddle point. The barrier along this coordinate is very small and on the order of the zero-point energy, leading to a red-shifted fundamental transition. To determine the extent of the red shift, one needs to solve the vibrational eigenvalue problem for this double minimum potential. For the present, it is observed that the simulated IR spectrum at the <sup>2</sup>A<sub>2</sub> saddle point agrees much better with the experimental IR-PD spectrum of V<sub>6</sub>O<sub>15</sub><sup>-</sup>, suggesting that the harmonic approximation for this particular vibrational mode breaks down completely and that the fundamental transition in question is not only red-shifted, but also loses considerably in intensity. A similar vibrational mode, also characterized by a double-minimum potential and a shallow barrier, is found for V<sub>8</sub>O<sub>20</sub><sup>-</sup> (see Figure 3.13). The effect on the IR-PD spectrum is, however, less pronounced in the latter case.

**V<sub>7</sub>O<sub>18</sub><sup>-</sup>** Four fragment ions, V<sub>3</sub>O<sub>8</sub><sup>-</sup> (V<sub>4</sub>O<sub>10</sub> loss), V<sub>5</sub>O<sub>13</sub><sup>-</sup> (V<sub>2</sub>O<sub>5</sub> loss), V<sub>4</sub>O<sub>10</sub><sup>-</sup> (V<sub>3</sub>O<sub>8</sub> loss), and V<sub>6</sub>O<sub>15</sub><sup>-</sup> (VO<sub>3</sub> loss), are detected after IR-PD of V<sub>7</sub>O<sub>18</sub><sup>-</sup>. The relative fragment ion yields at 1000 cm<sup>-1</sup> are 1, 0.1, 0.04, and 0.03, respectively. At this wavelength roughly 25% of the parent ions are depleted by the unattenuated FELIX beam. The IR-PD spectrum of V<sub>7</sub>O<sub>18</sub><sup>-</sup> measured by monitoring the dominant fragmentation channel, V<sub>4</sub>O<sub>10</sub> loss, is shown in Figure 3.11. V<sub>3</sub>O<sub>8</sub><sup>-</sup> is continuously produced in the spectral region from 1050 to 800 cm<sup>-1</sup>. Two maxima, associated with the vanadyl and V–O–V transitions, are found at 1004 and 871 cm<sup>-1</sup>, respectively. The IR-PD spectra of the other fragment ions are similar in shape, but with minor differences.

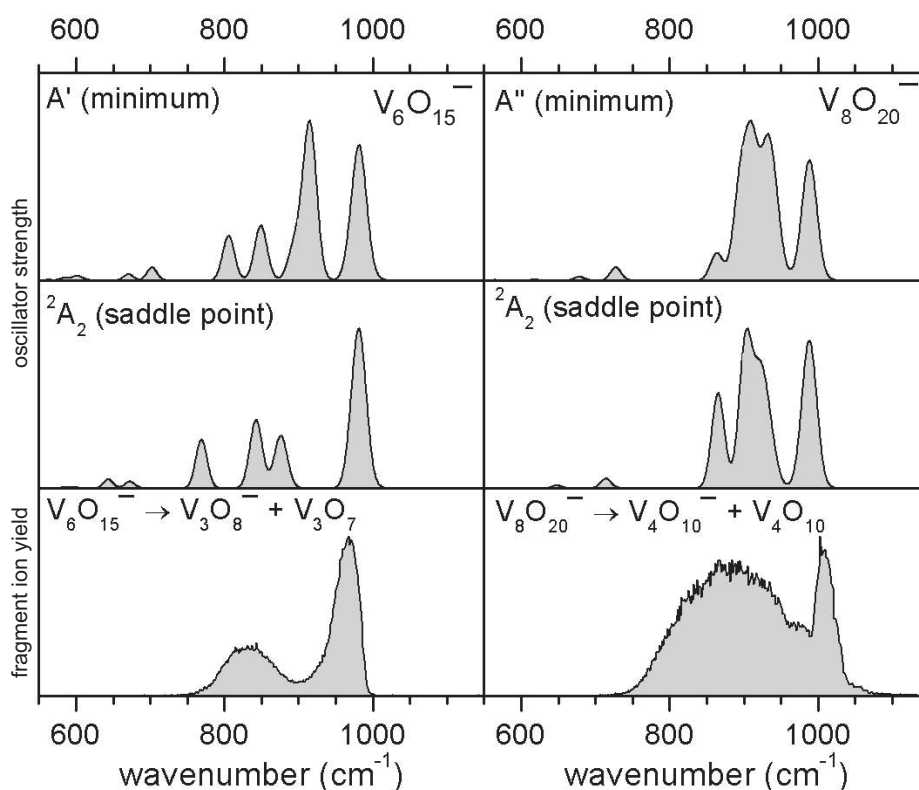


**Figure 3.13:** Simulated IR absorption spectra, based on scaled B3LYP/TZVP frequencies and oscillator strengths of the lowest energy isomer in its electronic ground state (top row) and an energetically low-lying first-order saddle point (middle row) for  $V_6O_{15}^-$  (left) and  $V_8O_{20}^-$  (right). The  ${}^2A_2$  saddle point connects two equivalent  $C_s$  structures through a  $C_{2v}$  transition state. The barrier along this coordinate is on the order of the zero point energy, leading to a red-shifted fundamental transition of this pronounced anharmonic vibration. The lower row shows the experimental IR-PD spectra for each parent ion.

The spectrum of the  $V_6O_{15}^-$  fragment ion shows an additional weak band at  $735\text{ cm}^{-1}$ , while the formation of the other fragment ions vanishes below  $800\text{ cm}^{-1}$ . In the spectra of  $V_5O_{13}^-$  and  $V_4O_{10}^-$  a weak signal is also observed above  $1040\text{ cm}^{-1}$ . The previous CID study [97] finds only two fragment ions, namely  $V_3O_8^-$  ( $V_4O_{10}$  loss) and  $V_5O_{13}^-$  ( $V_2O_5$  loss). This suggests that the fragment ions  $V_4O_{10}^-$  and  $V_6O_{15}^-$  are stable intermediates, which can fragment further and lose  $VO_2$  at higher excess energies.

The lowest energy structure found for  $V_7O_{18}^-$  is a pyramidal structure ( $C_{2v}$ ) but similarly to  $V_5O_{13}^-$  there is a second isomer with a bridged ( $C_s$ ) structure (see Figure 3.12). The energy gap between the two structures,  $0.27\text{ eV}$ , is larger than for  $V_5O_{13}^-$ , and the bridged isomer is not expected to contribute to the observed spectrum. The IR absorption spectrum of the pyramidal structure is characterized by

a strong absorption feature at  $990\text{ cm}^{-1}$  (seven  $\text{V}=\text{O}$  stretch modes), a very strong one around  $900\text{ cm}^{-1}$  (six  $\text{V}-\text{O}-\text{V}$  stretch modes) and a very weak absorption at  $683\text{ cm}^{-1}$ . This can explain the observed spectrum. However, the simulated spectrum of the bridged isomer (top of Figure 3.11) is very similar to that of the pyramidal isomer and the weak feature calculated at  $746\text{ cm}^{-1}$  for the bridged isomer is even closer to the observed weak feature at  $739\text{ cm}^{-1}$ . An unambiguous assignment is therefore in this case not possible.

$\text{V}_8\text{O}_{20}^-$  Four fragment ions of different mass are detected upon IR-PD of  $\text{V}_8\text{O}_{20}^-$ . The dominant photofragmentation channel is the formation of  $\text{V}_4\text{O}_{10}^-$  ( $\text{V}_4\text{O}_{10}$  loss), followed by the production of  $\text{V}_3\text{O}_8^-$  ( $\text{V}_5\text{O}_{12}$  loss),  $\text{V}_5\text{O}_{13}^-$  ( $\text{V}_3\text{O}_7$  loss) and  $\text{V}_6\text{O}_{15}^-$  ( $\text{V}_2\text{O}_5$  loss) with relative yields of 1, 0.02, 0.01, and 0.002, respectively, at  $1014\text{ cm}^{-1}$ . The IR-PD spectrum of the most abundantly formed fragment ion,  $\text{V}_4\text{O}_{10}^-$ , is shown in Figure 3.2. IR-PD spectra measured at the other possible fragment ion masses look very similar and are not shown. Two main features are observed; a narrow band in the vanadyl region of the spectrum at  $1004\text{ cm}^{-1}$  and a considerably broader band at lower energies with a maximum at  $871\text{ cm}^{-1}$ . With the full FELIX beam parent ion depletion of up to 85% is observed. The relative intensities yield an absorption cross section ratio of three to two for the  $1004\text{ cm}^{-1}$  and  $871\text{ cm}^{-1}$  band maxima.

The lowest energy structure found for  $\text{V}_8\text{O}_{20}^-$  is a distorted six-face cube structure (see Figure 3.8). Localization of the unpaired electron in the  $^2\text{A}'$  ground state leads to symmetry lowering from  $O_h$  to  $C_s$ . Of the eight vanadyl modes three contribute significantly to the vanadyl band at  $988\text{ cm}^{-1}$ , found at  $1004\text{ cm}^{-1}$  in the experimental IR-PD spectrum. The  $\text{V}-\text{O}-\text{V}$  bonds, which correspond to the edges of the  $\text{V}_8\text{O}_{20}^-$  cube combine to form the broad feature predicted at  $911\text{ cm}^{-1}$ . Five  $\text{V}-\text{O}-\text{V}$  modes contribute in the region from  $850$  to  $950\text{ cm}^{-1}$ , producing a broader feature, centered at  $856\text{ cm}^{-1}$ , with a width of  $\sim 60\text{ cm}^{-1}$ . The assignment of the  $871\text{ cm}^{-1}$  band in the experimental IR-PD spectrum to  $\text{V}-\text{O}-\text{V}$  modes is straightforward, however the width of the simulated band is less than twice that observed in the experiment. Note, similar to  $\text{V}_6\text{O}_{15}^-$  there also exist two equivalent  $C_s$  structures for  $\text{V}_8\text{O}_{20}^-$ , which are separated by a shallow barrier. This leads to a break down of the harmonic approximation also in this case and may contribute to the width of the very broad  $\text{V}-\text{O}-\text{V}$  band in the vibrational spectra of  $\text{V}_8\text{O}_{20}^-$ .

## 3.4 Discussion

### 3.4.1 IR Spectra

In previous vibrational predissociation studies on mono- and divanadium oxide cations three types of vibrational modes were identified in the region from  $600$  to  $1600\text{ cm}^{-1}$

and assigned to (i) supoxo- ( $\sim 1160\text{ cm}^{-1}$ ), (ii) vanadyl- ( $1060\text{--}910\text{ cm}^{-1}$ ) and the (iii) V–O–V vibrational modes ( $< 840\text{ cm}^{-1}$ ) [113]. A similar grouping of vibrational modes is observed for the vanadium oxide anions: (i) superoxo- ( $\sim 1100\text{ cm}^{-1}$ ), (ii) vanadyl- ( $1020\text{--}990\text{ cm}^{-1}$ ) and the (iii) V–O–V vibrational modes ( $< 900\text{ cm}^{-1}$ ). The modes for terminal V–O single bonds fall also into the latter range.

The intensities of the IR active modes range from weak ( $\sim 50\text{ km/mol}$ ) for the superoxo-mode in  $\text{V}_2\text{O}_7^-$ , to very strong ( $> 2000\text{ km/mol}$ ) for individual O–V–O modes in the largest cluster anions studied. In general, the V=O and O–V–O modes are of comparable intensities, except for  $\text{V}_4\text{O}_{10}^-$ , where the high symmetry of the cluster anion dominates the dipole selection rule, resulting in a comparably weak and red-shifted O–V–O band. Because the vanadyl stretching modes are limited to a narrower region of the spectrum, they generally overlap at the present spectral resolution and therefore produce a narrower and more intense band. The width of this vanadyl band remains similar through all IR-PD spectra, while the O–V–O band at lower energy gains considerably in width and relative intensity with cluster size. The increase in relative intensity is mainly due to an increase of the oscillator strength of the most intense O–V–O modes with cluster size, and only to a lesser degree, due to the increase (relative to the V=O modes) in the number of transitions.

Three general trends of the infrared absorption as a function of cluster size are observed in the IR-PD spectra of  $\text{V}_n\text{O}_m^-$  cluster. (i) With increasing number of vanadium atoms the absorption maximum of the vanadyl band shifts from  $950\text{--}960\text{ cm}^{-1}$  in divanadium oxide cluster anions by roughly  $+50\text{ cm}^{-1}$  to slightly above  $1000\text{ cm}^{-1}$  in  $\text{V}_7\text{O}_{18}^-$  and  $\text{V}_8\text{O}_{20}^-$ . This blue shift (see Figure 3.2) is well reproduced by the scaled B3LYP frequencies, which yield a shift of about  $+47\text{ cm}^{-1}$  in the convoluted spectra going from  $\text{V}_2\text{O}_6^-$  to  $\text{V}_8\text{O}_{20}^-$ . The only exception to this trend is observed in the IR-PD spectrum of  $\text{V}_6\text{O}_{15}^-$ , which exhibits an absorption maximum more than  $30\text{ cm}^{-1}$  to the red compared to the next smaller cluster anions containing five or four vanadium atoms. A genetic algorithm has been used to make sure that there is not a different isomer of  $\text{V}_6\text{O}_{15}^-$  with lower energy than the  $C_s$  cage structure shown in Figure 3.8 which could possibly explain this deviating position of the vanadyl band. (ii) With increasing cluster size the relative intensity of the absorption below  $\sim 800\text{ cm}^{-1}$  decreases. Also this trend is well reproduced by the calculations. (iii) For all clusters with  $n \leq 4$  the V–O–V absorption band ( $750\text{--}950\text{ cm}^{-1}$ ) is much broader and therefore also less structured than predicted by the simulated spectra. This effect is attributed to the non-harmonic nature of these modes, leading to considerable mode mixing and the appearance of combination bands. The excellent agreement of the spectra in Figure 3.14—discussed later—, suggests that this broadening is not due to the IR-MPD mechanism, otherwise it would not appear in the HREELS spectrum in Figure 3.14.

### 3.4.2 Confirmation of Cage Structures

The calculations convincingly confirm the first experimental identification of cage structure for all larger vanadium oxide cluster anions. The cages resemble highly symmetric, geometric forms like the tetrahedron ( $V_4O_{10}^-$ ), the tri-prism ( $V_6O_{15}^-$ ) and the cube ( $V_8O_{20}^-$ ) and were originally observed [94] or predicted [111] for neutral vanadium oxide clusters. However, the unpaired extra electron in the cages localizes in the larger cages  $V_6O_{15}^-$  and  $V_8O_{20}^-$  reducing their symmetry to  $C_s$ . Only for the smallest cage,  $V_4O_{10}^-$ , the unpaired electron is fully delocalized over the four (symmetry equivalent) vanadium atoms and the system shows the full  $D_{2d}$  symmetry. The consequence of this delocalization is clearly born out in the IR-PD spectra of  $V_4O_{10}^-$ ; in contrast to the larger anions with an even number of vanadium atoms it reveals no absorption in the 800–950  $\text{cm}^{-1}$  region. This transition from delocalized to localized electrons when going from  $V_4O_{10}^-$  to  $V_6O_{15}^-$  in the series of  $V_nO_m^-$  cluster anions is only correctly described when a hybrid functional with the right admixture of Fock exchange such as B3LYP is applied [104]. In contrast, BLYP (no Fock exchange) yields delocalization (and fully symmetric structures) for all three systems, whereas BHLYP (50% Fock exchange) enforces localization even with BHLYP. Comparison of the calculated IR spectra for all three functionals shows that B3LYP provides the right answer [104]. For further support, single point CCSD(T) calculations have been made (at the BHLYP equilibrium structures) for  $V_4O_{10}^-$  and  $V_6O_{15}^-$ . They confirm for  $V_4O_{10}^-$  that the  $D_{2d}$  structure has a lower energy than the  $C_s$  isomer, whereas for  $V_6O_{15}^-$  the  $C_{2v}$  structure has a higher energy than the  $C_s$  isomer. That an increasing admixture of Fock exchange (connected with increasing self-interaction correction) leads to an increasing tendency for electron localization has been found before [122, 123], but not always is B3LYP the right solution. For the case of electron holes in silica, BHLYP is needed to get the correct localization of the hole on one oxygen site [124].

$(V_2O_5)_n^-$  clusters with an even number of vanadium atoms consist of  $O=V(O-)_3$  units only and the anionic charge is connected with an extra electron in V d-states. In contrast, the cluster of type  $[(VO_3)(V_2O_5)_n]^-$  with  $n=1-3$  have a closed electronic shell and the extra electron is used to form a  $O=V^{(-)}(O-)_4$  or a  $(O=)_2V^{(-)}(O-)_2$  structure element. Nevertheless, the IR-PD spectra of both types of clusters are similar (see Figure 3.2).

The present results show a geometric transition as a function of vanadium oxide cluster size. Similar to the vanadium oxide cluster cations, the divanadium oxide cluster anions have “quasi-planar” structures, with a four-membered V–O–V–O ring. Vanadium oxide cluster anions with three vanadium atoms represent an intermediate cluster class; they show a three dimensional backbone structure, but still contain one vanadium atom that contributes only two bonds to the cage backbone.  $V_4O_{10}^-$  is the first cage structure, in which each vanadium atom forms three V–O–V bonds and

only a single terminal vanadyl bond. Most larger clusters follow this trend, making this structural element a general criterion for particular stable structure in vanadium oxide cluster anions.

The dominant fragmentation channels for the smaller ( $n < 4$ ) anions are loss of one or two oxygen atoms and formation of  $V_2O_5^-$  or  $V_3O_7^-$ . In the larger systems  $V_3O_8^-$  and  $V_4O_{10}^-$  are predominantly formed, identifying these two ions as particular stable building blocks for vanadium oxide cluster anions. Interestingly photodissociation and not electron detachment is observed to be the dominant “reaction” channel. For most of the clusters this observation is supported by the calculations (see Table 3.2) with the exception of  $V_4O_{10}^-$ , for which the electron affinity (4.49 eV) is calculated more than 1.2 eV below the lowest dissociation channel (5.74 eV).

### 3.4.3 Comparison with Crystal Surfaces

Even though the largest cluster anion studied here,  $V_8O_{20}^-$ , is still quite small, it reveals some striking similarities with the properties of a  $V_2O_5$  surface, making it an interesting candidate for studying surface adsorption and surface reactivity on a model system in the gas phase. In Figure 3.14 the IR-PD spectrum of  $V_8O_{20}^-$  is compared to the high resolution electron energy loss (HREELS) spectrum of a freshly cleaved  $V_2O_5$  single crystal surface [125], which also probes vibrational states. The spectra are surprisingly similar in the region above  $740\text{ cm}^{-1}$ , both displaying two bands of similar width and relative intensity. Their assignment is identical, i.e., to vibrational modes of singly- and doubly-coordinated oxygen atoms. The third broad band of the surface spectrum is not observed in the gas phase. This can easily be rationalized, because this band is assigned to triply coordinated oxygen sites, which do not exist in the  $V_8O_{20}^-$  cluster anion. Hence, the vibrational spectra reflect clearly the structural features that gas phase clusters and solid surfaces have in common (V=O and V–O–V bonds), but also the feature by which they differ (triply coordinated O).

### 3.4.4 Superoxo and Peroxo Groups

Peroxo (and also superoxo) groups are of interest because they play a role in the reoxidation of vanadium oxide species in catalytic processes, e.g. peroxo groups may be formed in the reoxidation of vanadium III to vanadium V sites,  $V^{III}(O^-)_3 + O_2 \rightarrow (O_2)V^V(O^-)_3$  [10, 126]. In an ionic picture, superoxo and peroxo groups correspond to  $(O_2)^-$  and  $(O_2)^{2-}$  species, respectively, with the additional electrons in antibonding p-p orbitals. Therefore, the O–O bond distance increases in the series (gas phase)  $O_2$ ,  $(O_2)^-$ , and  $(O_2)^{2-}$  and the vibrational frequencies decrease. Superoxo and peroxo species are expected to be present in gas phase species in which the oxygen content is larger than given by the highest oxidation state for vanadium,  $VO_{2.5}$ ,  $VO_2^+$ , or  $VO_3^-$ .

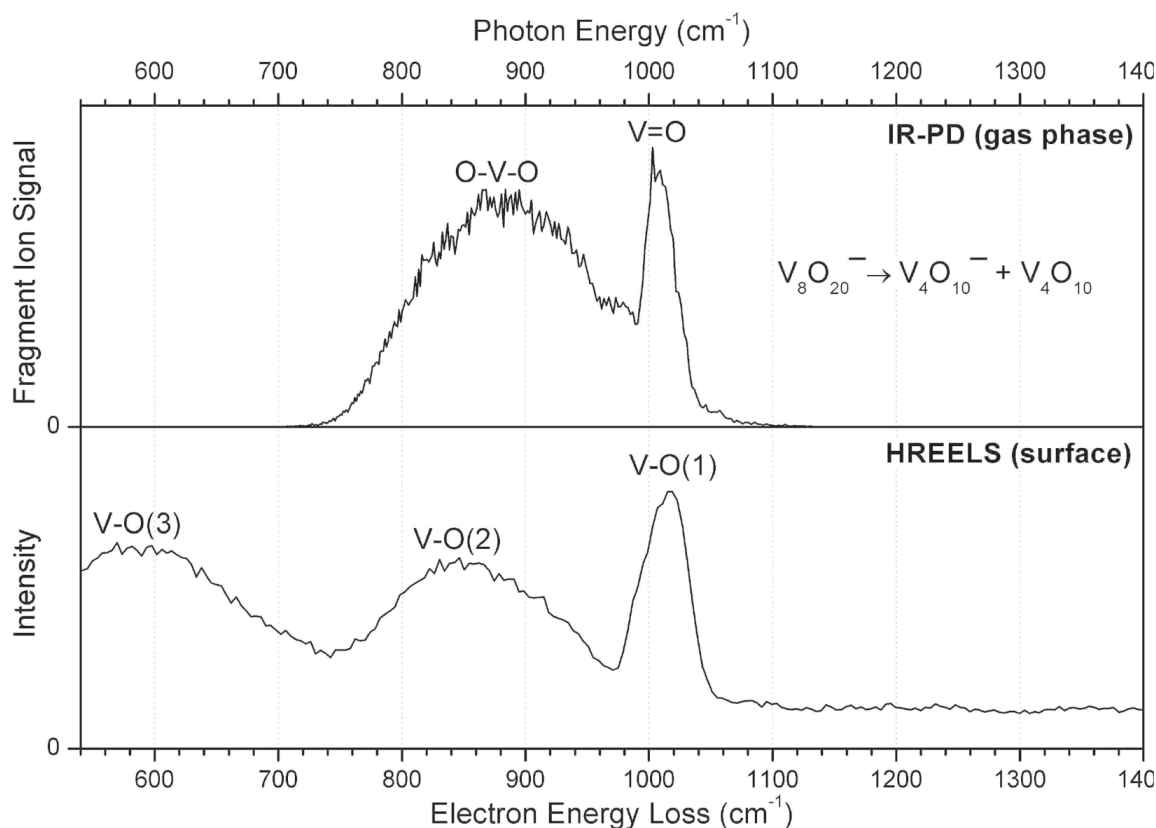


**Figure 3.14:** Vibrational spectra of different forms of vanadium oxide. The IR-PD spectrum of the gas phase cluster anion  $\text{V}_8\text{O}_{20}^-$  (top) and the spectrum of a freshly cleaved 001 surface of  $\text{V}_2\text{O}_5$  (bottom) [125], measured using high resolution electron energy loss spectroscopy, are shown.

Examples are  $\text{V}_2\text{O}_6^+$  and  $\text{V}_2\text{O}_7^-$  for which superoxo vibrations are found at  $1160 \text{ cm}^{-1}$  (Ref. [113]) and  $1112 \text{ cm}^{-1}$  (this study).

A particular interesting case is  $\text{V}_4\text{O}_{11}^-$ . Formally, the neutral  $\text{V}_4\text{O}_{11}$  cluster is obtained by replacing a  $\text{O}^{2-}$  with an  $(\text{O}_2)^{2-}$  ion in the  $\text{V}_4\text{O}_{10}$  cage. When the replacement is made in a  $\text{V}-\text{O}-\text{V}$  bridge, either a  $\mu-(\eta^2:\eta^2)$ -peroxo or a  $\mu^2$ -peroxo group is obtained.<sup>1</sup> The latter is 0.05 eV less stable. When a vanadyl oxygen is replaced the  $\eta^2$ -peroxo group described before [103] is obtained, which, however, is 0.23 eV less stable. (DFT studies have also been made for  $\mu-(\eta^2:\eta^2)$  and  $\eta^2$  peroxo groups on the  $\text{V}_2\text{O}_5$  (001) surface [128].) What happens if an electron is added to the different

<sup>1</sup> $\mu$ : In inorganic nomenclature: “An affix used in names to signify that a group so designated bridges two or more centers of coordination” [127].  $\eta$  (or hapto): In inorganic nomenclature: “An affix giving a topological indication of the bonding between a p-electron ligand and the central atom in a coordination entity. A right superscript numerical index indicates the number of ligating atoms in the p-electron system of the ligand which bind to the central atom” [127].

$V_4O_{11}$  peroxo isomers? In  $V_4O_{10}$  as in all vanadium oxides with vanadium in the +V oxidation state, the lowest unoccupied states are vanadium 3d-states. In peroxo compounds, antibonding O (2p-2p) states are also available among the low-lying unoccupied states. If an electron is added to the V d-states of the  $\mu$ -( $\eta^2$ : $\eta^2$ ) peroxo isomer, it either distributes among the four V sites resulting in a symmetric  $C_{2v}$  structure or it localizes at one of the neighboring V sites resulting in a  $C_s$  structure with different bond distances from the two neighboring V sites to the peroxo unit (Figure 3.10). On the B3LYP/TZVP potential energy surface, the former ( $C_{2v}$ ) structure is a saddle point and only the latter ( $C_s$ ) is a minimum. However, CCSD(T) single point calculations indicate that this symmetry breaking may be an artifact of B3LYP. The  $\eta^2$ - and  $\mu^2$ -isomers of  $V_4O_{11}^-$  have even higher energies than the  $\mu$ -( $\eta^2$ : $\eta^2$ ) peroxo isomer. Upon adding an electron to the  $\eta^2$ - and  $\mu^2$ -isomers of  $V_4O_{11}$ , the extra electron occupies d-states at the V-site connected to the peroxo unit in the  $\eta^2$ -isomer, whereas in the  $\mu^2$ -peroxo isomer it is on one of the V sites “opposite” to the peroxo unit.

However, lower energy  $V_4O_{11}^-$  isomers are obtained if the electron is added to the antibonding (p-p)  $\sigma^*$  orbital of the  $O_2$  unit. In the case of the  $\mu$ -( $\eta^2$ : $\eta^2$ )-peroxo isomer, formally a  $(O_2)^{3-}$  species, “peroxoanion”, is created with a bond order of 0.5 compared to 1.0 in  $(O_2)^{2-}$ . This explains the long O—O bond of 2.04 Å in this  $\mu$ -( $\eta^2$ : $\eta^2$ ) “peroxoanion” isomer with  $C_{2v}$  structure (Figure 3.10). CCSD(T) calculations show that this is the second most stable isomer of  $V_4O_{11}^-$ .

In the case of the  $\mu^2$ -peroxo isomer, adding an electron to the antibonding (2p-2p)  $\sigma^*$  orbital of the O—O unit, opens the V—O—O—V bridge completely and the lowest energy dioxo structure shown in Figure 3.10 is obtained. In summary, conversion of the neutral cluster into a cluster anion induces a qualitative change in the structure and the peroxo group is no longer a structural feature of the most stable  $V_4O_{11}^-$  isomers. As CCSD(T) calculations indicate, the second and third most stable isomers feature an  $O_2$  unit in  $\mu$ -( $\eta^2$ : $\eta^2$ ) configuration, with the additional electron either in the  $O_2$  unit or in d-states, i.e.,  $\mu$ -( $\eta^2$ : $\eta^2$ ) “peroxoanion” ( $C_{2v}^{-2}B_2$ ) or  $\mu$ -( $\eta^2$ : $\eta^2$ ) peroxo ( $C_{2v}^{-2}A_1$ ), respectively.

Although the existence of the two lowest energy isomers of  $V_4O_{11}^-$ , dioxo-bridge and  $\mu$ -( $\eta^2$ : $\eta^2$ ) “peroxoanion” finds a simple explanation in adding the extra electron to antibonding orbitals of the peroxo group of the neutral parent compound,  $V_4O_{11}$ , the structure search was originally limited to the different peroxo structures known from the neutral  $V_4O_{11}$  cluster. Only the insufficient agreement of the observed IR spectrum with the one predicted for the lowest peroxo structure, the  $\mu$ -( $\eta^2$ : $\eta^2$ ) peroxo isomer (Figure 3.9), was the motivation to apply a global optimization scheme. This scheme has generated the two lowest energy structures for  $V_4O_{11}^-$ . Even with the genetic algorithm, there is no guarantee that the global minimum structure is found. It is therefore important that the IR-PD spectrum has been measured which is in sufficient agreement with the B3LYP prediction for the “DIOXO” structure, thus confirming that the latter may be indeed the global minimum structure.

fragment	O	O <sub>2</sub>	VO <sub>2</sub>	VO <sub>3</sub>	VO <sub>3</sub> <sup>-</sup>	V <sub>2</sub> O <sub>5</sub>	V <sub>3</sub> O <sub>8</sub>	V <sub>4</sub> O <sub>10</sub>	VDE
<b>parent ion</b>									
V <sub>2</sub> O <sub>6</sub> <sup>-</sup>	<b>3.93</b>	4.75		5.26	5.26				5.70
V <sub>2</sub> O <sub>7</sub> <sup>-</sup>	3.05	<b>1.79</b>							5.55
V <sub>3</sub> O <sub>8</sub> <sup>-</sup>	<b>5.53</b>		6.32	<b>6.40</b>	<b>6.35</b>	6.35			6.08
V <sub>4</sub> O <sub>10</sub> <sup>-</sup>	6.04		<b>5.74</b>			6.92			4.49
V <sub>4</sub> O <sub>11</sub> <sup>-</sup>	<b>2.05</b>	2.90		<b>3.95</b>		5.04			6.66
V <sub>5</sub> O <sub>13</sub> <sup>-</sup>			6.91	<b>4.90</b>	5.24	<b>5.42</b>			
V <sub>6</sub> O <sub>15</sub> <sup>-</sup>			<b>5.16</b>			<b>4.84</b>			5.28
V <sub>7</sub> O <sub>18</sub> <sup>-</sup>				<b>4.99</b>		<b>4.92</b>	<b>5.01</b>	<b>3.81</b>	
V <sub>8</sub> O <sub>20</sub> <sup>-</sup>						4.87		<b>3.18</b>	5.48

**Table 3.2:** Calculated fragmentation energies and vertical detachment energies (VDE), in eV. Bold numbers correspond to observed fragmentation channels.

## 3.5 Summary

IR-PD spectra of collisionally cooled, mass-selected vanadium oxide cluster anions are measured ranging from V<sub>2</sub>O<sub>6</sub><sup>-</sup> to V<sub>8</sub>O<sub>20</sub><sup>-</sup> and cluster structures are identified through a comparison with simulated IR spectra based on harmonic frequencies and intensities from DFT calculations. In general, the agreement between simulated *linear* IR spectra and experimental *multiple photon absorption* IR-PD spectra is sufficient to identify a single electronic and structural isomer responsible for the main absorption features. In several cases (V<sub>2</sub>O<sub>6</sub><sup>-</sup>, V<sub>4</sub>O<sub>11</sub><sup>-</sup>, V<sub>5</sub>O<sub>13</sub><sup>-</sup>, and V<sub>7</sub>O<sub>18</sub><sup>-</sup>) additional isomers may be present, leading to additional, weaker absorption features. For V<sub>6</sub>O<sub>15</sub><sup>-</sup> and V<sub>8</sub>O<sub>20</sub><sup>-</sup> evidence for a breakdown of the harmonic approximation is found. This study shows that only the interplay between experiment and theory allows for a structural characterization of these species and that either experiment or theory alone is not sufficient.